Spatiotemporal Distribution Of Ionospheric Irregularities Over India During St. Patrick's Day Storm

Rajat Acharya*, Randhir Singh & Radhika Chipade

Space Applications Centre, Ambawadi Vistaar, Ahmedabad, Gujarat 380 015, India

The irregularities formed over the equatorial ionospheric region over the Indian sector have been studied for the first time for the day of the most intense geomagnetic storm of solar cycle-24, which occurred on 17.03.2015, using Rate of TEC Index (ROTI) as the index for the study. These values have been derived using the measurements done with the TEC network receivers of the Indian SBAS system, GAGAN. Spatial and temporal variations of ROTI have been observed and compared to the same parameters on a quiet day with occurrence of nominal scintillation. The latitudinal symmetry of the irregularities for a given local time was evident. It has been found that the ionospheric irregularities formed over this region get immensely enhanced due to the storm in terms of its intensity and spatial extent, as well. The temporal spread of the irregularities has been observed and the statistical variations of the occurrences were compared with respect to those on quiet days. The results have provided few interesting observations including an understanding of the profundity and extensiveness of the irregularities and of the possibilities of consequent scintillation for the navigation signal over Indian region during space weather induced intense geomagnetic disturbances.

Keywords: Equatorial Ionosphere, Space weather, St. Patrick's Day Storm, ROTI, Scintillation

1 Introduction

The earth's ionosphere is sensitive to the events induced by the space weather components like the solar wind. It shows variations in its electron density distribution and total electron content when affected by suchfactors. The solar wind carries with it the interplanetary magnetic field (IMF) which impinges on the earth's magnetosphere on the day side. When the z component, Bz of the IMF, defined typically in geocentric solar ecliptic (GSE) frames, abruptly turns southward, the associated electric field enters the Earth's ionosphere at the polar latitudes through the reconnected and open geomagnetic field lines. This field instantaneously penetrates up to the equatorial ionosphere and is referred to as prompt penetration electric field (PPEF). Similarly, when the IMF Bzturns northward, an effective electric field in the opposite sense is experienced at the equatorial latitudes due to the over-shielding effect[1]. The PPEF is eastward in the dayside while westward in the night side of the globe and the over shielding field is just in the opposite sense. However, they both last for the typical time scale of the order of tens of minutes.

Along with the PPEF, intense variations in the geomagnetic field, called geomagnetic storm, may occur during the southward polarity of the IMF Bz. In addition, there occurs substorms at the polar latitudes which may, in turn, also alter the equatorial electric field [2,3,4,5]. Apart from these, the disturbance dynamo, occurring after an intense storm and driven by equatorward thermospheric wind, can affect the equatorial electric field by generation of a westward electric field on the dayside and eastward electric field on the night side [6,7].

When an enhancement of the eastward electric field is caused due to any of the above reasons, it modifies the E x B force acting on the equatorial ionospheric plasma and responsible for the vertical drift. When the field is enhanced, plasma, in large excess than the nominal, is lifted vertically up at the equatorial region and gets transported across the latitudes through diffusion at these elevated heights. Such increment in the plasma at these higher altitudes may lead to a top-heavy condition in the ionosphere after the local sunset, as the normal photo generated electron density at comparatively lower heights, diminishes rapidly due to faster recombination rates. This leads to the formation of Gravitational Rayleigh Taylor instability[8](RTI) in the plasma. As a result, the top denser plasma penetrates downwards, diffuses through and sometimes engulfs the plasma below of lower density forming a bubble-like structure. This

Corresponding Email: rajat_acharya@ sac.isro.gov.in

causes random local variations in the plasma density or irregularities. These irregularities, in turn, lead to very sharp variations in the refractive index which results in rapid fluctuations in the amplitude and phase of the signals passing through it, causing Scintillations. To quantify the irregularities, Pi *et al.*[9] introduced a term called Rate of TEC Index (ROTI). It signifies the depth of irregularities over the natural variations of the ionospheric TEC. Rate of TEC Index (ROTI) maps derived from ROT are used as a standard measure to monitor impact of space weather on the Earth's ionosphere. Recently, the International GNSS Service (IGS) accepted ROTI maps as a new ionospheric product[10].

In this work, we have observed the spatiotemporal variations of the ionospheric irregularities, which are quantified by the ROTI values, the latter being defined in Sec. 2.4. The ROTI has shown a good correlation with the amplitude scintillation index, S4. Therefore, ROTI can statistically be used as a proxy for the occurrence of the amplitude scintillation. The observed spatial and temporal distributions on the day of the storm event will provide us with the understanding of the time periods and the regions of possible disruptions in the navigation services over the Indian region during severe geomagnetic storms along with their probable intensities. For the purpose of the study, we have compared the extent and depth of the ROTI formation on the storm day with those for a quiet day, on the same month. These comparisons directly indicate the extent of the storm in both spread and depth while giving us an idea of its unusual severity.

2 Materials and Methods

2.1 Effect of ionospheric disturbance on navigation

Scintillation is the rapid fluctuation in the signal amplitude and phase as they pass through the irregularities in the ionosphere. During the scintillation, the GNSS users in low latitudes can experience substantial deterioration in code and carrier phase ranging, hence degraded levels of accuracy in stand-alone positioning. Scintillation can be severe enough that the C/N_0 of the received GPS signal drops below the receiver's locking threshold, forcing the receiver to reacquire the signal [11]. As a result, the continuity of the system is greatly affected. Amplitude scintillation is measured by the S4 index, and is expressed in terms of the signal intensity as [12]

$$S_4{}^2 = \frac{<I^2>-<I>^2}{<I>^2} \qquad \ldots 1(a)$$

where 'I' is the intensity of the signal and <> is the expected value. Therefore, S4 is essentially a normalized standard deviation in the signal intensity estimated typically over 60 seconds period. The features of the amplitude scintillation over Indian region are described in Acharya *et al.* [13]. The other form of scintillation, i.e., the phase scintillation occurs from rapid phase variations in the signal may lead to cycle slips and loss of lock for receivers as they track the signal. Phase scintillation is quantified by σ_φ, the standard deviation of the detrended phase over an interval of up to 60 seconds and is expressed as[12]

$$\sigma_\varphi = \sqrt{< \varphi^2 > \; - < \varphi >^2} \text{ radians} \qquad \ldots 1(b)$$

where, φ is the detrended phase of the received signal. However, the amplitude and the phase scintillations are highly correlated [14]. Therefore, characterization of any one of them provides a fair understanding of that of the other. Scintillation has a fair correlation with the irregularity index ROTI.

In this work, we have observed the spatiotemporal variations of the ionospheric irregularities, which are quantified by the ROTI values, defined in Sec. 2.4. The ROTI has shown a good correlation with the amplitude scintillation index, S4. The relevant researches in this regard have been mentioned in the Sec. 2.5. Therefore, ionospheric irregularity index ROTI can statistically be used as a proxy for the occurrence of the amplitude scintillation.

It is evident now that, for the occurrence of irregularities, formation of plasma instability, initiated by top heavy condition of the plasma, is a necessary condition. Therefore, it occurs typically after the local sunset in the evening and continues till post-midnight period in equatorial regions. In the Indian sector, this predominantly occurs during the equinoctial seasons when the pre-reversal enhancement (PRE) is conspicuous and aids the formation of the instability. However, during geomagnetic storm, it may even occur during other times of the day and other parts of the year, as well. The observed spatial and temporal distributions on the day of the storm event will provide us with the understanding of the time periods and the regions of possible disruptions in the navigation services over the Indian region during severe geomagnetic storms along with their probable intensities.

2.2 St. Patrick'sDay storm

In this paper, we focus on the ionospheric responses to the geomagnetic storm that occurred on 17–18 March 2015. This geomagnetic storm is more

popularly known as the St. Patrick's Day storm. It was the largest one occurring during solar cycle 24. There were two severe Coronal Mass Ejections (CME) on March, 15, 2015 that occurred between 0200 – 0230 hrs UT. The two successive large eruptions that left the sun were directed toward Earth with the trailing one moving faster than the leading one. So, they joined up while speeding through space, causing what is known as co-rotating Interaction region (CIR) in the solar wind. When this region of the solar wind impinged upon the earth's magnetosphere, it had a maximum speed of about 680 km/s. The resultant shock compressed the magnetosphere with consequent SSC at around 0430 UT. The z component of the interplanetary magnetic field, Bz was southwardly from around the same time and continued to remain so for the next few hours. The duration of the storm was about 18 hours out of which the G3 and G4 conditions sustained for 12 hours [15]. The plots of the IMF, Bz and Dst on this day is shown in Fig. 1 (a and b) respectively. It is important to note that the IMF Bz turned southwards around 0600 hrs and then again at around 1200 hrs and this time it was followed by a G4 level geomagnetic storm. An effective electric field of 200 mV/km were measured to get induced during the event.

For the purpose of the study, we have compared the extent and depth of the ROTI formation on the storm day and compared them with those for a quiet day, on the same month. These comparisons directly indicate the extent of the storm in both spread and depth while giving us an idea of its unusual severity.

2.3 GAGAN TEC Network

This work has been done using select TEC data from the TEC measuring receivers of the Indian SBAS system, GPS Aided GEO Augmented Navigation (GAGAN) over India. GAGAN has an independent network of dual frequency receivers for the measurement of ionospheric total electron content (TEC). This network, called the TEC network, is for the purpose of modelling the ionosphere over the Indian equatorial region and its anomalous features. For the purpose, very precise and sensitive dual frequency receivers are primarily installed at 26 different airports in a noise surveyed and multipath free environment. The locations of these GAGAN TEC receivers across India are shown in Fig. 2.

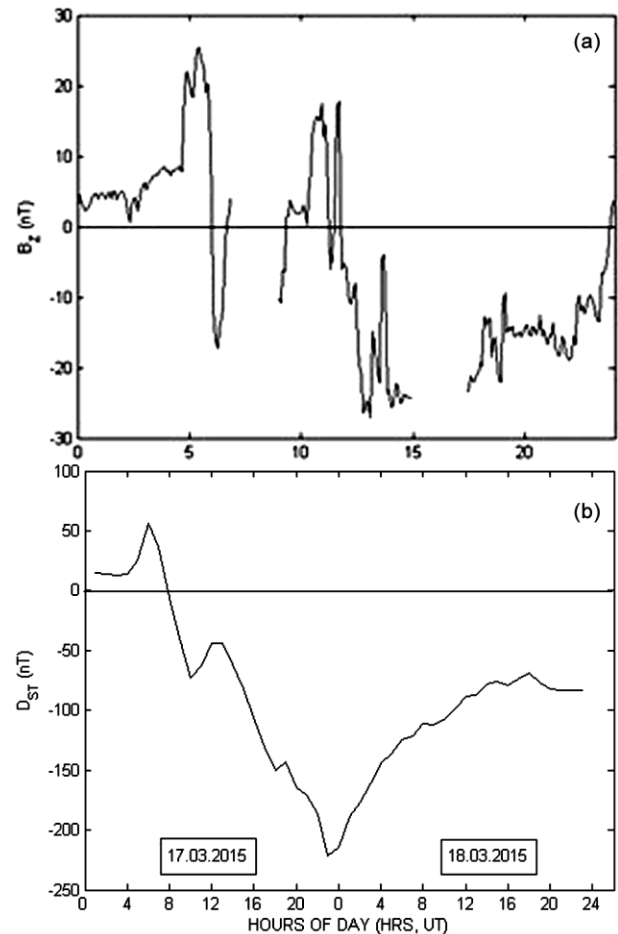These receivers provide the TEC values along the slant signal path for each GPS satellite visible in TEC

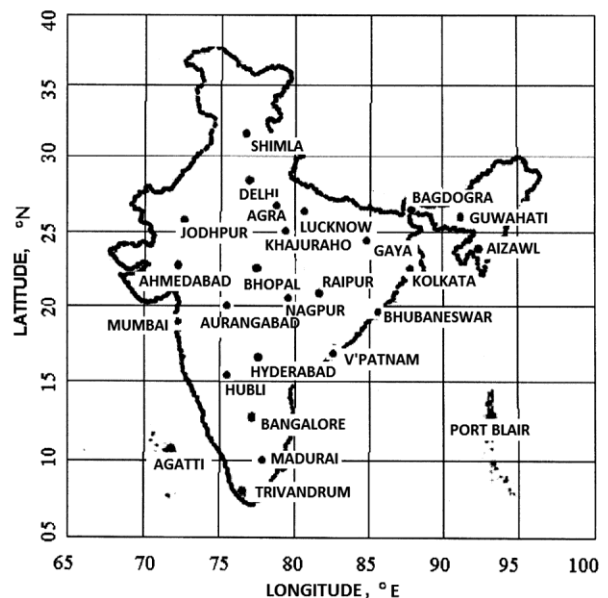Fig. 1 — (a) IMF-Bz and (b) Dst variations on St. Patrick's Day (17.03.2015)

Fig. 2 — Locations of GAGAN TEC Stations

units with corresponding elevation, azimuth and time stamps at the interval of 30 seconds. TEC are recorded in these receivers in TEC units (TECU), where, 1 TECU = 10^{16}electrons/m^2. In addition, these receivers are also capable of estimating the amplitude scintillation at L1 in terms of S4 index [12]. Measurements are recorded up to a lowest elevation of 15° making chances of noise and multipath related deterioration of the received signals practically negligible. However, in our study, we have discarded all the measurements below 20° elevation to avoid any perturbation due to extensive multipath component, which can influence ROTI estimates, other than ionospheric variations.

2.4 Estimation of ROTI

For a satellite navigation signal traversing from the orbiting satellites to the dynamic user, a portion of the signal passes through the ionosphere and experience the delay due to it. The delay is given by

$$\delta = 40.3 \ T/f^2 \qquad \qquad ...(2)$$

where δ is the total ionospheric delay in terms of equivalent excess path in metres, T is the TEC along the signal path in electrons/m^{2}and f is the frequency of the signal in Hz. The variations measured in this delay occur as the ionosphere changes with time and the signal changes its path with time, as well. Therefore, both the spatial and temporal change in the ionospheric electron density affect it. The overall effect observed by the signal can be quantified by the Rate of TEC (ROT). Therefore, the ROT can be mathematically represented as

$$ROT = dT/dt = \partial T/\partial t + \dot{v}\,\partial T/\partial s \qquad ...(3)$$

where, $\partial T/\partial t$ represents the temporal change in the ionosphere and $\partial T/\partial s$ is its spatial change and v is the velocity of the point where the signal ray intersects the effective height of the ionosphere. This point is called the ionospheric pierce point (IPP). The location of the IPP is given in terms of the receiver location and the elevation angle as[16]

$\lambda =$ asin (sin $\lambda_s$cosψ + cos λ_s cos z sin ψ)

$\phi = \phi_s +$ asin (sin ψ sin ξ / cos λ)

and $\psi = \pi/2 - \xi - \sin \left(\frac{R_e}{R_e + h}\cos \xi\right)$ ...(4)

where, λ is the latitude of the IPP and ϕ is its longitude. λs and ϕs are the latitude and longitude of the station respectively and ξ is the elevation angle. Re is the radius of the earth and h is the effective ionospheric height, taken typically as 350 km.

The ROTI values are derived using the time series of the TEC values obtained from these dual frequency GAGAN receivers after they are converted to TEC units. First, the TEC values, ordered in time, are used to derive the time series of the Rate of TEC (ROT). The ROT, defined in Eq. (3) is derived from the measured TEC data as,

$$ROT_k = \frac{TEC_k - TEC_{k-1}}{t_k - t_{k-1}}\text{TECU/min} \qquad ...(5a)$$

where, ROT_k is the ROT value derived at the time instant t_k and TEC_k and TEC_{k-1} are the measured TEC value at the time instant t_k and t_{k-1} respectively. Once the ROT values are derived, these values obtained over a 5 minutes' window period are utilized to find ROTI, which is assigned to the time instant at the edge of the window and to the corresponding IPP location. The change in the ionospheric TEC experienced by the signal is mostly systematic. However, whenever, there is an irregularity in the ionosphere, the ROT values change abruptly. Such changes can be captured by the index called ROT Index (ROTI) by measuring the deviations in the time rate of change in TEC over the systematic variations, along a signal path. So, ROTI is nothing but the standard deviation in the TEC rate over an interval of 5 minutes [9]. It is defined as

$$ROT_k = \frac{TEC_k - TEC_{k-1}}{t_k - t_{k-1}}\text{TECU/min} \qquad …(5b)$$

where, ROT is the Rate of TEC along the signal path expressed in TECU/minute. The occurrences of the irregularities and hence the ROTI is both is both geographically and temporally variable. The 11-year solar cycle, season of the year, and geomagnetic location all play a role in degree of activity [17].

During the estimation, all elevations below 20°have been disregarded to avoid any influence of multipath. To focus on the effect over the Indian region, all IPP points beyond 65°E and 100°E longitude are also removed. Although, the measurement interval is 30 seconds, some of the measurements were found missing due to the loss of lock of the receivers. To eliminate these points, the data where the time intervals between the successive measurements are more than 120 seconds were removed from deriving the ROT. Since ROT was derived by using the difference of successive measured TEC values, any interfrequency bias present therein does not affect the result.

Eq. 3 shows that the slant ROT measured using the satellite signal moving through the ionosphere, consists of two terms. These two terms are described below.

(i) The first term represents the variation of TEC, solely with time, for a definite fixed location. This is mainly due to the change in electron density at the location occurring with time in the interval between two successive measurements, as a result of appreciation or depreciation of photogeneration or transport of the plasma, in this period. This component is typically systematic in nature.

(ii) The second term arises due to the change in the path that the signal traverses through the ionosphere, in the interval between two successive measurements. This again results from two factors,

a. The difference in the "path length" through the ionosphere of the signal for the two successive measurements. This change is also systematic and can be shown to be negligible for the threshold elevation angle and for the measurement interval used here.

b. Difference in the spatial profile of the electron density along different paths. It is this term that captures the effect of spatial irregularities present in the electron density in a given snapshot period, as the signal traverses through them with time. This term is important in our case.

Many researchers have worked elaborately on these components of ROTI. Among them, important to mention are, Shimna and Vijayan[18], Wilken et al.[19], Jakowski and Hoque[20] and many others, who proposed efficient new algorithm to remove the effects of the spatial gradients related to non-uniformity of the inter IPP distances on vertical ROTI values. On the other hand, Jakowski et al.[21], Nesterov et al.[22], Juan et al.[23], Ma et al.[24] and many others, worked to separate out the effects of time variations and relative motion of the ionospheric disturbances with respect to the signal path and derived new indices for the same. They studied the fine structure of the ionospheric irregularities and their movements using these indices.

However, in our case, out of these components mentioned above, the systematic terms in (i) and (ii – a) remain low and approximately unaltered in each of the measurements, within the period of one ROTI observation. As ROTI is derived as the standard deviation of the individual ROT, the constant terms appearing in each of the components get cancelled.

As a result, only the random variation in spatial distribution of electron density, i.e., the component in (ii – b), makes the most significant contribution and is conspicuously present in measured ROTI. Further, during the storm, this irregularity values are so large, that they override any other smaller variations. Therefore, the ordinary ROTI values on this day, without any further corrections, can effectively captures the spatial irregularities.

2.5 Correlation of ROTI and S4

Various researchers have contributed in obtaining and understanding the relationship between ROTI and scintillation, like Pi et al.[9], Basu et al.[25], Liu and Radicella[26] and many others. It has been reported by earlier researchers that the trends of ROTI and S4 corresponds well during the generation, evolution, and decay phase of amplitude scintillation. Basu et al.[25] reported that ROTI measurement can be used to predict the presence of scintillations causing those irregularities, although the quantitative relationship between them varies considerably. Xiong et al.[27] estimated the correlation coefficient between ROTI and S4 for different seasons and had shown that there is a good correlation in summer and winter compared to spring and autumn seasons. Yang and Liu[28] found the correlation coefficient between ROTI and S4 to vary from 0.6 to near 0.8 under different geomagnetic conditions. So, ROTI has been used extensively as a proxy to the ionospheric scintillation, particularly over the low latitudes[29,30,31]. Recently, Acharya and Majumder[32] established a statistical relationship between the occurrence of ROTI and S4 in which they have shown that for a given ROTI value, the S4 variation over the Indian equatorial region shows log-normal distribution.

The ROTI values, derived from the TEC data measured by the TEC receivers at the stations, are observed for the storm day, i.e. 17th March, 2015. In order to compare the storm effect with respect to a nominal quiet day, similar observations are also carried out for a quiet day of the month, 10th March, 2015. The dates were chosen in the same equinoctial month to keep other factors approximately unaltered. Each ROTI value obtained is tagged with its corresponding time and the IPP location. This location is estimated using Eq. 4. Due to the diversified locations of the stations, and due to the fact that the GPS satellites are moving with time, the IPP locations will appear at different coordinates over the earth across the time. At any instant, the IPP

generated at different longitudes will have different local times. Since ionospheric properties are local time specific, the ROTI values, generated at different IPP locations are ordered in terms of their longitudinal local time. Finally, this sorted data of ROTI values are used and analysed for their spatiotemporal properties. The observed features and their comparative studies are described in the section 3.

3 Results and Discussions

3.1 Local time snapshots of the irregularities

The ROTI values for a definite time interval are derived from all the available IPP points and plotted. Fig. 3 shows the contour plot of the ROTI values derived from the individual IPPs obtained at their respective locations and at definite local time snapshot,starting from 1500 hrs LT till 2100 hrs LT on the storm day, 17th March, 2015.

For each of these figures, an inclusion window of 1800 seconds was considered from the snapshot instant to form a batch of data from which the contour is derived. Cubic interpolations were carried out wherever necessary. Since, most of the receivers are located over the Indian landmass, for the given cut-off angle, the IPP points are located mostly on the Indian mainland or at locations adjacent to the land boundary. Further, due to the geographical structure of India, the receivers installed within the longitudinal range of 75°E to 80°Eare extended along the longitude across the centre of the Indian mainland to a maximum extent. These data, therefore, can be used to observe the continuous variation across the region of our interest with the maximum density of the IPP points. Hence, the reliability of the data and any statistical inference drawn out of it is also the maximum here. Therefore, to observe the characteristics of the spatiotemporal variations, spatial filters are applied to the derived data with the
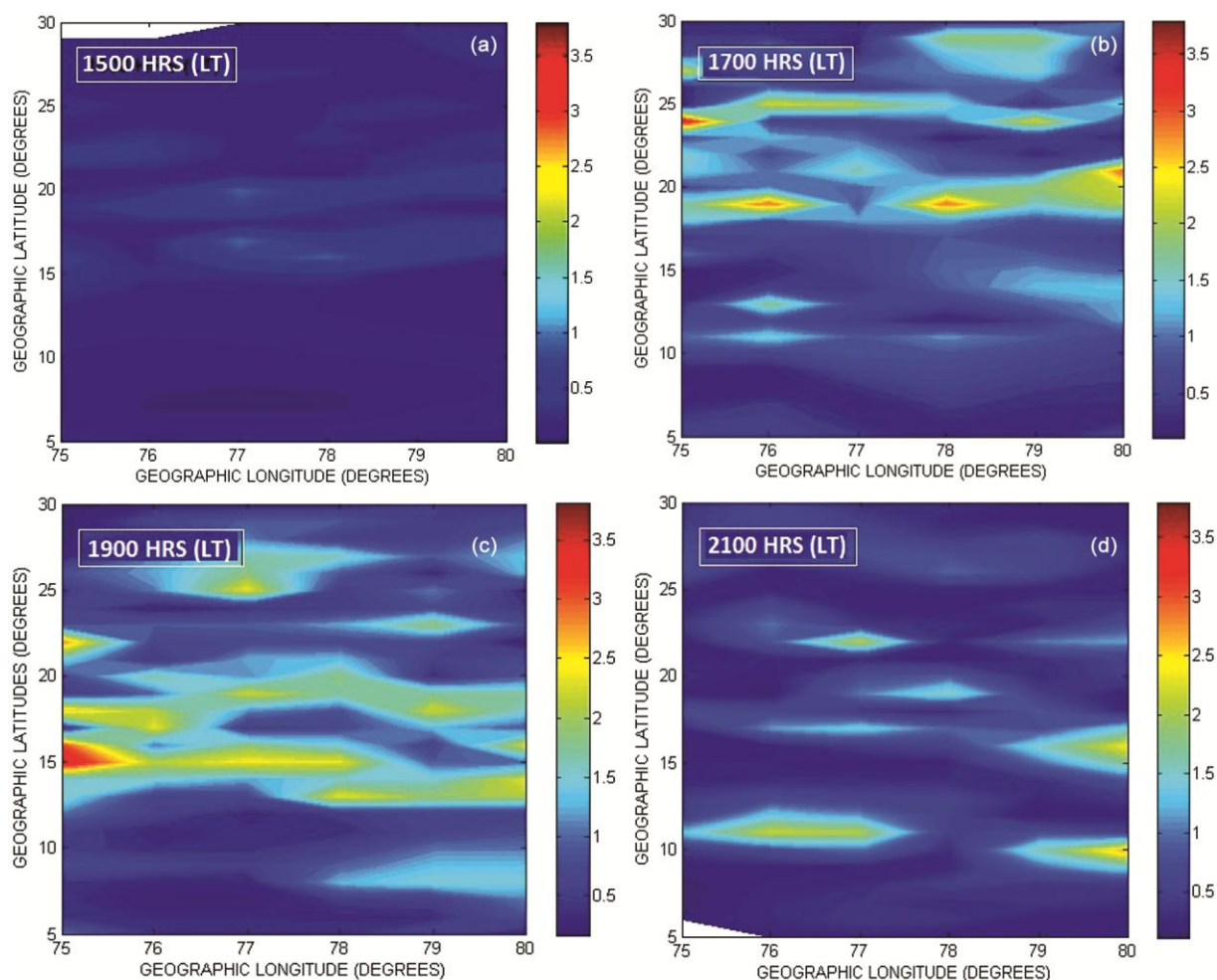

Fig. 3 — Spatial distribution of ROTI on the 17.03.2015 at (a) 1500 hrs (b) 1700 hrs (c) 1900 hrs, and (d) 2100 hrs

boundary defined by the longitude at 75°E and 80°E and by latitude 05°N and 40°N.

The plots distinctly reveal the latitudinal layered structure i.e., stratified nature of the irregularities. The similarity of the ROTI values along any definite latitudes over this region for any particular local time, while significant variations are observed across the latitudinal direction. This was expected since the driving factors for the ionospheric irregularities are the local time, the declination of the location and the pre-sunset condition of the electron density gradient which again are dependent upon the geomagnetic latitude. So, for a given local time, considering the fact that over the entire Indian region, the declination does not change significantly, it is only the latitude that determines the ionospheric variation. Further, considering the different local time snapshots shown in Fig. 3, irregularities in terms of the ROTI intensity, shows a systematic variation over time. We shall point out more interesting temporal characteristics of the irregularities in the next section, where we discuss the spatiotemporal plots.

3.2 Spatiotemporal Variations of the irregularities

It is evident from the discussions in Sec. 3.1 that, for a given local time, approximately identical values are expected for the same latitude with variations only across the latitudes. Therefore, for any particular local time, only one representative ROTI value can be sufficiently used as the representation of the ionospheric irregularity at any definite latitude. In our study, the ROTI value for given latitude is derived from the maximum of the values observed at that latitude over the longitudinal extent between 75°E to 80° E. As a result, we can plot the latitudinal variation of ROTI and its variation over local time in a 2-dimensional plot. Such a spatiotemporal plot is shown in Fig. 4 (a and b).

The variations of the archetypal ROTI values for different latitudes are shown along the y axis while the temporal variations in terms of the local time are shown along the x axis. The discrete time interval taken between values along the time axis is 30 minutes while the latitudinal resolution is 0.5°. However, the spatiotemporal contour is generated out of these discrete values to represent the variations in a smooth and continuous manner. In these plots, the ROTI values are in TECU/min unit and are represented by the colour as indicated by the colour map. This enables us to understand the spatiotemporal variation of ROTI in a single plot. Fig. 4(a) shows the

plot for the storm day, i.e. 17th March, 2015, while Fig. 4(b) represents a quiet day of the same month, which is 10th March, 2015.

It is easily observable from the plots that, on the selected quiet day of 10th March, 2015, the ROTI values have reached a maximum of only about 1.2 TECU/min around 21 hrs, LT for a small time period of about 30 minutes. The maximum values were observed at around 12°N latitude with latitudinal extent of about 2 degrees. On the other hand, on the storm day of 17th March, 2015, considerably high ROTI values started showing from 1830 hrs LT at the same location of around 12° latitude. This was within a period of 1 hour from the time when the IMF Bz turned southward for the second time. Incidentally, this is also the period for PRE, which remains predominant over the Indian region during the considered month. Moreover, unlike the quiet day, the irregularities have rapidly extended primarily towards
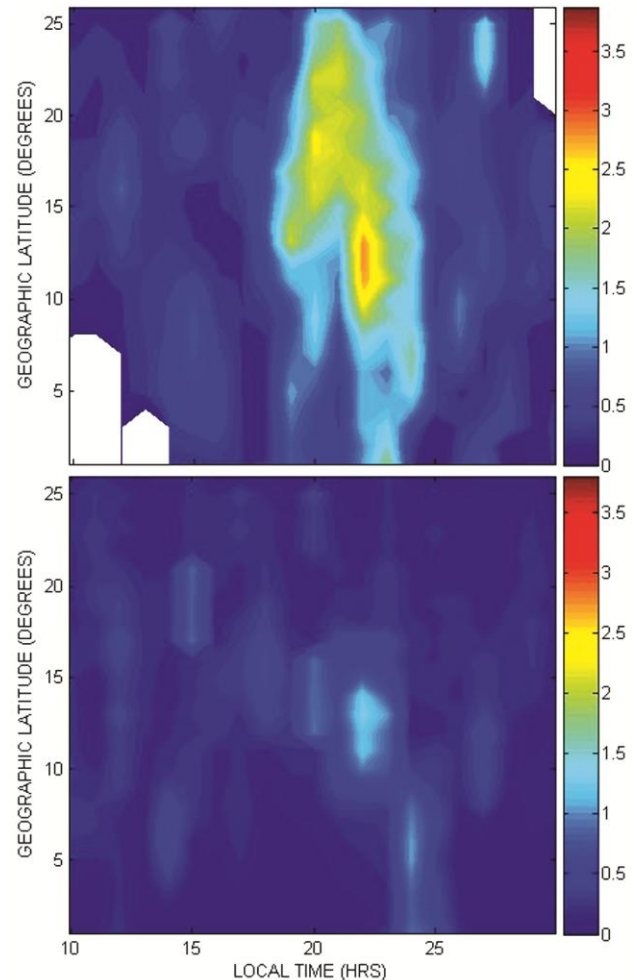

Fig. 4 — Spatio-temporal distribution of ROTI on (a) Storm Day 17.03.2015, and (b) Quiet Day 10.03.2015

north and reached till the highest latitude of 25°N by 2030 hrs LT, i.e. within a time span of around 2 hoursfrom the first occurrence of the irregularities. Not only it has reached to such high latitude of 25°N, which is typically unusual, but a very high ROTI value of around 2.5 TECU/min was observed over these extensive regions, which continued for more than 2 hours. This characterises the severity of the storm effect. After 2100 hrs LT, the irregularities gradually started moving off towards south. Around 2200 hrs LT, the maximum ROTI value of 3.6 TEC/min was observed at around 12°N latitude. The latitudinal extent of this highest ROTI values spread about 2 degrees and continues for around 30 minutes. After this, the irregularities gradually reduced in strength and receded, reaching southward up to around 5°N latitude. When compared with the quiet day, there were obvious escalations in the values in terms of intensity of the ROTI and its spatial extent for the storm day. The highest ROTI value of 3.6 TECU/min on the storm day was about 3times compared to the highest value of 1.2TECU/min. on the quiet day. Interestingly, the highest range of values of ROTI on the storm day were formed at around the same location, maintained over the same latitudinal extent of around 2° and remained for the same time of around 30 minutes as those for observed for the quiet day. This is evident from the Fig. 4 (a and b).

However, no significant irregularities were observed after the local midnight, although there were substorms of moderate strength occurring during these hours[33]. However, this is consistent with the observation by Basu *et al.*[25] that, during post-midnight period, there is a steep decay in small scale irregularities and ROTI does not remain associated with detectable levels.

3.3 Statistical comparison of irregularities

The comparison with the highest attained ROTI value only may not give the complete impression of

the situation. In the last section, it was observed from the result that on the storm day higher ranges of ROTI values were retained for much more extended time compared to the occurrence times of equiprobable values on a nominal quiet day. In order to bring out these features, it is necessary to view the distribution of the different probabilities of occurrences of the ROTI values over these different days and compare them. Therefore, we have plotted the 50, 20, 10 and 1% exceedance values of the ROTI as a function of time for different latitudinal regions. At any given instant and for a given extent of location, the exceedance value for p% is that value of ROTI which is exceeded only for p% in total probability, for that specific time when all occurrences in that particular location range is considered. In other words, it is the ROTI value, R in the probability density distribution of ROTI over the region and time of concern, for which $100 \times \int_R^\infty P(x)dx = p$, where P is the probability density function of the occurrence of ROTI. The multiplication factor 100 is to convert the proportional value in the integral to percentage. Three different latitudinal regions were considered, (a) the equatorial region, ranging from 0° to <14° N geographic latitude, (b) the crest region, extending from 14°N to <28°N geographic latitude and (c) the hyper-crest region, for geographic latitudes more than 28° N. The corresponding plots are shown in Fig. 5 (a – c) for the storm day and Fig.6 (a – c) for the quiet day.

Comparing the plots in Fig. (5 and 6), it is evident that, not only the maximum value, but the overall ROTI intensity has been raised on the stormy day compared to a quiet day. In comparison to the quiet day, the 50% exceedance values remained almost the same. Therefore, occurrences of 50% of all the lowest values of ROTI did not change significantly between these two days. However, it is to be noted here that,
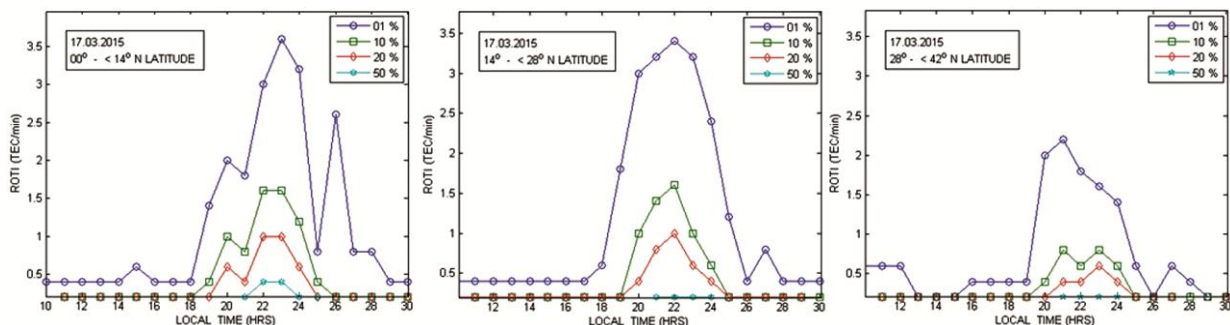

Fig. 5 — Exceedence Plots for different percentages of ROTI occurrence on Storm Day 17.03.2015 (a) Equatorial region (00 - < 14 N Latitude) (b) Crest region (14 - <28 N Latitude), and (c) Hypercrest region (28 - < 42 N Latitude)
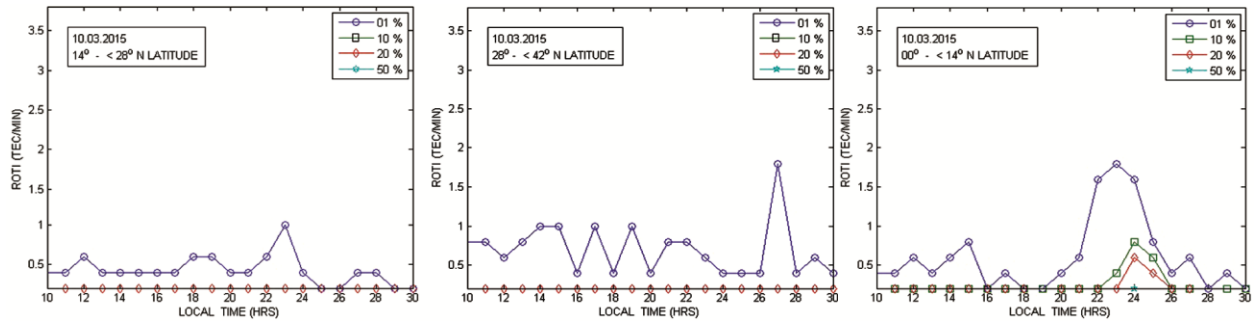
Fig. 6 — Exceedence Plots for different percentages of ROTI occurrence on Quiet Day 10.03.2015 for (a) Equatorial region (00 - < 14 N Latitude) (b) Crest region (14 - <28 N Latitude), and (c) Hypercrest region (28 - < 42 N Latitude)

these are the points constituted by ROTI values around 0.2 TECU/min. The lower exceedance percentages, on the contrary, have much higher ROTI values than other days in comparison. In other words, the highest 1% of the ROTI, which exceeded only 2TECU/min on a quiet day, have exceeded 3.5 TECU/min on the storm day. The highest 10% of all occurrences exceeded is around 0.85 TECU/min on a quiet day while on the storm day this value remained around 1.6 TECU/min. This is evident from Fig. 5 (a and b). A huge enhancement at the crest region is also observed on the storm day compared to the quiet day.

The temporal continuation period is indicated by the width of each curve in the plot. As far as they are concerned, the 1% exceedance value remained above 1.5 TECU/min for more than 7 hours on the storm day while that interval is about 2.5 hours for the quiet day. Similarly, exceedance of 2 TECU/min remained for more than 2 hours on the storm day while it did not occur at all on the quiet day. Therefore, the major characteristic of the irregularities, showing enhancement in intensity, extent over region and the continuation over time, distinctly appear on the plot for the day of the St. Patricks day storm.

3.4 Observations

In this section, we discuss the few interesting and important observations obtained in our result. Prominent amongst the other features which are observed from the plots for the equatorial region, is the fact that the chosen intense storm initiated large irregularities within 1 hour from the instant of the southward turning of the IMF Bz. The time of occurrence is not only earlier than the time of commencement for quiet days but is almost coincident with the local sunset time in the month considered. This points out to the fact that the penetrated electric field was exceptionally intense that

within a period of one hour, it has driven the plasma to an extent and magnitude that within a few minutes from the sunset, the vertical gradient became high enough to initiate the instability.

Also associated with this observation is the fact that since the dates chosen for analyses are those of the equinoctial period, pre-reversal enhancement (PRE) is expected at the local sunset hours. On the storm day, the southward turning at around 1200 hrs UT, i.e., around 1750 hrs LT on Indian longitudes, intensified the pre-reversal enhancement. Therefore, the large increment in the pre-reversal eastward electric field occurred due to the prompt penetration of electric field which worked in conjunction with the F layer dynamo electric field. Hence, such intense storm development at sunset sector produced significant modification in the vertical drift during the PRE and in turn, aided the formation of the early RT instability leading to the associated irregularities. However, on comparison with the quiet day, which also showed PRE occurrence, it is clear that on the storm day most of the irregularities were driven by the storm induced field, rather than that due to the F region dynamo.

A new and rather interesting point in the present set of results is that, the intense irregularity, showing up first near the crest region just after the storm onset, extended first towards north to reach up to more than 25° N latitude. But, after about 3.5 hours from the commencement of the storm, it moved southward considerably before subsiding. One of the possible reasons that can result in this southward drive of the plasma irregularities may be the prevalent southward thermospheric wind. It is well known that when large amount of energy is dissipated in the polar region during the geomagnetic storm, it results in conspicuous changes in the thermodynamic equilibrium in the upper atmosphere due to Joule's heating. This leads to the expansion of the neutral

atmosphere and results in equator ward neutral wind, mostly in the form of Travelling Atmospheric Disturbances (TAD), which ultimately cause the disturbance dynamo at the equatorial region[34]. Both the observations and model demonstrate that the TAD propagate equator ward with a phase speed of ~600-650 m/sec.[35]. These TADs will sweep the irregularities and with the mentioned speed would take approximately a little more than 3 hours to reach from the polar latitudes to the locations in question. This exactly matches to our time of occurrence.

Another interesting observation mentioned in Sec. 3.2 is that, for the storm day, the highest range of values of ROTI on the storm day were formed at around the same location, maintained over the same latitudinal extent of around 2° in latitude and remained for the same time of around 30 minutes, as observed for the highest values of irregularities on the quiet day. The formation of the irregularities has its origin on how fast large volumes of plasma get transported to the higher latitudes. The latter again is dependent upon the vertical drift velocity at the equatorial region. This observation indicates that the electric field generated by the eastward prompt penetration, occurring during the onset of the storm, does not change the average vertical drift velocities of the plasma observed on a quiet day and formed by the F region dynamo. However, they appear to increase the scatter in the drift velocity values, on both higher and lower sides of the average. It is the plasma with the spread components of the drift velocity due to the PPEF, which resulted in the early RTI and late extended components of the irregularity, while the unaltered average drift constitute the highest region of the irregularity occur at the same place and with same extension on both the selected quiet and storm day.

Finally, the storm induced irregularity continues up to midnight and then diminishes rapidly. This corroborates the observation of many earlier researchers like Basu *et al.*[25] and others etc. who attributed this phenomenon to the steep decay in small scale irregularities during post-midnight period.

4 Conclusions

We have observed and analysed the features of the irregularities generated as a result of the response of the equatorial ionosphere for the most intensive magnetospheric storm of cycle 24, on March 17, 2015, popularly known as St. Patricks Day storm.

This storm is associated with the transit of an intense CME through the Earth's magnetic field.

The spatiotemporal variations of the ionospheric irregularities over the Indian region, due to this huge storm are observed. The statistical variation of the probability of occurrences of different levels of irregularities over different distinct regions of the Indian equatorial region was also examined.

The irregularities were identified and quantified by the popularly used ROTI index. Few interesting results concerning the timing, location, intensity and the spatial extent of the irregularities have come out from the present study, by comparing the ROTI indices during the storm and on a quiet day with scintillation.

The main conclusions of this study are the following:

i. Intense geomagnetic storm generates ionospheric irregularities. For the storm selected in this work, the irregularities started within 1 hour from the instant of the southward turning of the IMF Bz, i.e., the condition which finally led to the formation of the storm.

ii. There is a strong similarity in the ROTI values for a given local time along any definite latitude across India.

iii. The initiation of the intense irregularity originates at the latitudinal location of the anomaly crest and expands with time first towards north and then towards southward directions.

iv. Intense storm creates irregularities that have the highest magnitude of about three times than that on a quiet day. The irregularities extend spatially much beyond the region covered by the irregularities during a nominal quiet day and linger for much more time than the equiprobable irregularity of a quiet day in terms of ROTI.

v. For the St. Patrick Days storm, the equiprobable values of the ROTI compared with the quietest day of the month, the intensity enhanced by about 3 times in the equatorial region. This enhancement exists in the anomaly crest region and in the hyper crest region, though the enhancement factor is much lesser in the latter.

vi. When the temporal extent is considered, the equiprobable values on the storm day linger for about three times than those on a quiet day.

vii. Interestingly, the few highest values of the irregularities attained on both quiet and storm days were found to be formed around the same

location, maintained over the same area and remained for around the same time interval.

viii. On the storm day, most of the irregularities were driven by the storm induced field, rather than that due to the F region dynamo of the PRE.

ix. The continuity of the storm induced irregularity continues up to midnight and then diminishes rapidly.

To conclude, it has come out in a conclusive manner that severe storm like that occurred on the St. Patrick's Day, can cause larger magnitude of irregularities and hence scintillation. Severe storm can affect extensive areas, otherwise considered to be unaffected over the Indian region. Further, severe storm can linger up to larger time extent. Therefore, it is necessary and important to identify the profundity and extensiveness of the irregularities and hence of the consequent scintillations of any navigation signal on the basis of the intensity of the geomagnetic disturbance. Further aspects of the low-latitude ionospheric response to diverse conditions of the magnetospheric disturbances form very good candidates for under investigation.

Acknowledgement

References

1   Kelly MC, Earth's Ionosphere: Plasma Physics and electrodynamics (Academic Press, USA),(2009) 126

2   Kikuchi T, Hashimoto KK, Kitamura TI, Tachihara H & Fejer B, *J Geophys Res,*108/A11 (2003) 1406.

3   Gonzales C A, Kelley MC, Fejer BG, Vickrey JF& Woodman RF, J*Geophys Res*, 84/A10 (1979) 5803.

4   Sastri, JH, Kamide Y & Yumoto K, *J Geophys Res*, 108/A10 (2003) 1375.

5   Huang CS, Foster JC, Goncharenko LP, Reeves GD, Chau JL, Yumoto K & Kitamura K, *J Geophys Res*, 109 (2004) A05219.

6   Blanc M& Richmond AD, *J Geophys Res*, 85 (1980) 1669.

7   Fuller-Rowell TJ, Cordrescu MV& Araujo-Pradere EA, *Capturing the storm-time F region ionospheric response in an empirical model in Space Weather,* in Geophysical Monograph, vol 125, edited by P Song, H Singer&G Siscoe (AGU, Washington D.C.) (2001) 393.

8   Huang CS, Kelly MC & Hysell DL, *J Geophys Res*, 98/A9 (1993), 15631.

9   Pi X, Mannucci A J, Lindqwister U J & Ho C M, *Geophys Res Lett*, 24 (1997), 2283.

10 Cherniak I, Krankowski A & Zakharenkova I, *GPS Solut*, 22 (2018), 69.

11 Doherty P, Ionospheric Scintillation Effects in Equatorial and Auroral Regions, *Proc ION GPS-2000* (Institute of Navigation, Utah) (2000) 662.

12 Fremouw EJ, Leadabrand RL, Livingstone RC, Cousin MD, Rino CL, Fair BC & Long RA, *Radio Sci,*13/1 (1978) 167.

13 Acharya R, Nagori N, Jain N, Sunda S, Regar S, Sivaraman MR & Badyopadhyay K, *Indian J Radio Space Phys*, 36 (2007), 394.

14 Moraes AO, Costa E, Abdu MA, Rodrigues FS, de Paula ER, Oliveira K & Perrella WJ, *Radio Sci,* 52 (4) (2017), 439.

15 https://www.swpc.noaa.gov/noaa-scales-explanation

16 Minimum Operational Performance Standards for GPS/ WAAS Airborne Equipments, RTCA,(DO-229B)(1999) A-34.

17 Basu S, MacKenzie E & Basu Su, *Radio Sci,*23/3 (1988), 363.

18 Shimna K & Vijayan MSM, *J Atmos Sol Terr Phys*, 209 (2020), 105400.

19 Wilken V, Kriegel M, Jakowski N & Berdermann J, *J Space Weather Space Clim*,8(2018), A19.

20 Jakowski N, Hoque MM, *Space Weather*, 17(2) (2019), 339.

21 Jakowski N, Borries C & Wilken V, *Radio Sci* 47(4) (2012), RS0L14.

22 Nesterov IA, Andreeva ES, Padokhin AM, Tumanova YS & Nazarenko MO, *GPS Solut*, 21(4) (2017), 1679.

23 Juan JM, Sanz J, Rovira-Garcia A, Gonzalez-Casado G, Ibanez D & Perez RO, *J Space Weather Space Clim*, 8(2018) A14.

24 Ma G, Li Q, Li J, Wan Q, Fan J, Wang X, Maruyama T & Zhang J, *J Atmos Sol TerrPhys*, 211(2020) 105485.

25 Basu S, Groves KM, Quinn JM & Doherty P, *J Atmos Sol Terr Phys,* 61 (16) (1999), 1219.

26 Liu Y & Radicella S, *Ann Geophys*, 147 (2019) 1.

27 Xiong C, Stolle C & Luhr H, *Space Weather*, 14 (2016), 563.

28 Yang Z & Liu Z, *GPS Solut,* 20 (4) (2016), 815.

29 Bagiya MS, Iyer KN, Joshi HP, Thampi SV, Tsugawa T, Ravindran S, Ravindran R & Pathan BM, *J Geophys: Space Physics,* 116 (2011) A01303.

30 Raghunath S &Ventaka Ratnam D, *Indian J Radio Space Phys,* 45 (2016) 11.

31 Abe OE, Villamide XO, Paparini C, Ngaya RH, Radicella SM & Nava B, *Ann Geophys,* 35 (2017) 1.

32 Acharya R & Majumder S, *Adv Space Res*, 63(6) (2018) 1892.

33 http://wdc.kugi.kyotou.ac.jp/ae_provisional/201503/index_20150317.html

34 Richmond AD & Matsushita S, *J Geophys Res: Space Physics,* 80 (19) (1975) 2839.

35 Lee CC, Liu JY, Chen MQ, Su SY, Yeh HC & Nozaki K, *J Geophys Res,* 109 (2004) A0930.